Drop impact on hairy surfaces

Alice Nasto, P.-T. Brun, and A. E. Hosoi

Phys. Rev. Fluids **4**, 064004 — Published 26 June 2019

DOI: 10.1103/PhysRevFluids.4.064004

Drop impact on hairy surfaces

Alice Nasto,[1] P.-T. Brun,[2] and A. E. Hosoi[1,3]

[1]*Department of Mechanical Engineering, Massachusetts Institute of Technology, Cambridge, Massachusetts 02139, USA*
[2]*Department of Chemical and Biological Engineering, Princeton University, Princeton, New Jersey, 08544, USA*
[3]*Department of Mathematics, Massachusetts Institute of Technology, Cambridge, Massachusetts 02139, USA*

We investigate the impact of liquid drops on millimeter-scale hairy surfaces. By varying the speed of the drop, the spacing of the hairs, and the viscosity of the liquid, we observe a variety of behaviors. In some cases, the liquid drop can remain on top of the hair after impact, similar to a Cassie-Baxter superhydrophobic state. If the drop penetrates the hairy surface, the hairs can resist droplet spreading. Using this scenario as a reference case, we rationalize the role of the hairs in dissipating the kinetic energy of the impacting drop through a balance of inertia, viscosity, and surface tension. The various observed behaviors are classified according scenarios in which kinetic energy is insufficient or in excess of this reference scenario, an argument that allows us to build and rationalize a phase diagram.

I. INTRODUCTION

It is well known that patterning a substrate with a microscale texture can make the surface superhydrophobic and lead to unusual drop impact dynamics, such as bouncing [1–3]. Such surfaces have been observed in nature on *Morpho* butterfly wings [4] and lotus leaves [5] for the purpose of quickly shedding water drops. Micropatterned surfaces also have been shown to be useful in a variety of engineering applications, such as anti-icing [6, 7], anti-condensation [8], or self-cleaning [9].

The spreading of a drop on a microtextured superhydrophobic surface can be limited by either capillarity or by viscosity [3, 10]. In the capillary limited regime, the maximal deformation of the drop is $D_{\max} \sim D_0 We^{1/4}$, where D_0 is the initial diameter of the drop and the Weber number, characterizing the relative size of inertial and capillary effects, is defined as $We = \rho V^2 D_0/\gamma$, where ρ is the density, V is the velocity of the impact and γ is the surface tension [3]. In the viscosity limited regime, the maximal deformation is given by $D_{\max} \sim D_0 Re^{1/5}$, where the Reynolds number, characterizing the relative size of inertial and viscous effects, is defined as $Re = \rho D_0 V/\mu$, where μ is the viscosity [3, 10]. In both these regimes, the lengthscales associated with the microscale texture are irrelevant.

Though patterned substrates in drop impact studies are typically microscale [2, 3, 11], interesting drop impact phenomena are also observed with larger features, such as wires [12], meshes [13, 14], pores [15] deformable substrates [16, 17] and chemically patterned domains [18]. Here we explore drop impact on what we refer to as a "mesoscale" texture, that is millimetric in size. In contrast to microscale textures, we find that the geometric features of the mesoscale hairy texture in our study are the most relevant lengthscales in determining the interfacial and viscous effects during drop impact. Our study investigates hairy textures which are at scales that are relevant to those found in natural systems benefiting from interactions with liquid drops. For example, plants in arid environments use hairs or spines to collect wind-blown fog [19–21]. There is an interest in emulating this behavior through the engineering of structures for fog harvesting in arid environments where water is scarce [22–24]. Additionally, similar hair-like textures can dissipate the kinetic energy of a liquid stream resulting in an anti-splash effect [25]. Here we explore the various impact scenarios observed with such textures and rationalize the physics of drop capture in hairy textures. Similar to our study, there have been studies on drop impact on porous media in which the lengthscales of the texture are relevant in the analysis of the penetration of the drop. In the Ryu *et al* study of drop impact through a mesh [13], the momentum of the droplet is balanced with the effect of Laplace pressure in the pore, though viscous effects are negligible. In contrast, our study is conducted in the viscosity dominated regime as well as the surface tension dominated regime, revealing a different mechanism for kinetic energy dissipation. In the Lorenceau *et al* study of a drop impacting a sieve [15], which considers the simplified case of a drop impacting a single pore and pushing through past a critical velocity, there is a balance of inertial, capillary, and viscous effects, giving rise to Reynolds and Weber numbers that similarly contain lengthscales relevant to the size of the pore. We use a similar approach to this relatively simplified case and extend it to to describe hairy surfaces.

II. EXPERIMENTAL SETUP

A schematic of our drop impact experiment with a hairy surface is shown in Fig. 1a. The hairy surfaces are cast from PDMS elastomer (with Young's modulus E = 2 MPa) using laser cut acrylic molds [26]. The hairs are shaped like slender truncated cones with an

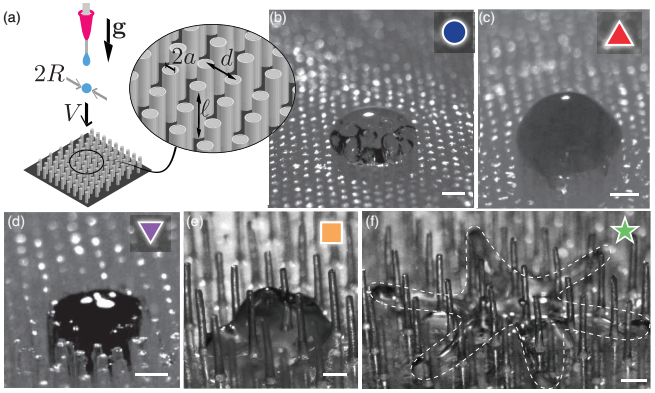

FIG. 1. a) Schematic of the drop impact experiment and the geometry of the hairs. b) Drop not penetrating the hairy texture on impact (glycerol, d = 0.5 mm, V = 0.6 m/s) c) A drop that partially penetrates the hairy texture (water d = 0.5 mm, V = 0.6 m/s). d) Drop that penetrates the surface and is "captured" and prevented from spreading (water d = 0.75 mm, V = 0.6 m/s) e) Drop that penetrates and spreads (water d = 2 mm, V = 0.6 m/s) f) Drop that penetrates and forms long fingers and ejects droplets (water, d = 2, V = 1.4 m/s). The dashed white line outlines the contours of the fingers of the drop. The scale bars indicate 1mm in all images.

average diameter of $e = 0.3$ mm and a length of $\ell = 2.7$ mm and are arranged in a hexagonal pattern with a center-to-center spacing d ranging from $d = 0.5$ mm to $d = 2$ mm (shown in Fig. 1a). Drops are formed by ejecting liquid through a needle (Nordson Precision, pink tips with inner diameter 0.61 mm) using a syringe pump at a slow rate of 0.5 μl/s to ensure quasi-static drop formation. The drops have a radius of $R = 1.5 \pm 0.08$ mm. The liquids used in the experiment are water (with viscosity $\mu = 8.9 \times 10^{-4}$ Pa $\cdot$ s), a 1:1 glycerol/water mix ($\mu = 8.8 \times 10^{-3}$ Pa $\cdot$ s), a 4:1 glycerol/water mix ($\mu = 0.09$ Pa $\cdot$ s), and glycerol ($\mu = 0.75$ Pa $\cdot$ s). The height of the needle is changed to vary the speed of the impact V (ranging from $V = 0.55$ m/s to $V = 2.3$ m/s). The drop impact is filmed at a rate of 3600 fps. For each experiment, the impact speed and drop radius is measured from the videos.

Depending on the combination of parameters – the spacing d, the impact speed V, and the liquid properties (viscosity μ, density ρ, and surface tension σ) – different behaviors are observed and classified into one of five scenarios, shown in Fig. 1. One scenario is the drop not penetrating the hairs upon impact. A representative experiment demonstrating this is shown in Fig. 1b and Supplemental Movie 1 (see Ref. [27]), denoted by ○. This case is similar to a Cassie-Baxter state [28] that is often observed for superhydrophobic textured surfaces. A drop can partially penetrate the hairy texture, as shown in Fig 1c (denoted by △) and Supplemental Movie 2 (see Ref. [29]). In this case, part of the drop is submerged in the texture, and part of it remains on top. For a drop that penetrates through the texture, it can be "captured," which we define as not spreading beyond the hairs that the drop touches at the moment of impact, as shown in Fig. 1d and Supplemental Movie 3 (see Ref. [30])) (denoted by ▽). The drop adopts a cylindrical shape while trapped between the hairs. This drop capture phenomenon is unique to mesoscale textures and is not observed for microscale textures [1–3, 11]. In cases where the drop is not captured after penetrating through the hairy surface, it can either spread past the hairs but remain as one drop (shown in Fig. 1e and Supplemental Movie 4 (see Ref. [31]), denoted by □), or it can form fingers as it pushes between hairs and break up into multiple droplets (shown in Fig. 1f and Movie 5 (see Ref. [32]), denoted by ★).

III. THE MODEL

In our experiments, inertial, viscous, and surface tension effects are expected to play a role in the impact dynamics. A range of parameters is explored to capture behavior in the viscous limit and the inviscid limit. The respective magnitude of the viscous and surface tension effects is captured by the capillary number, defined as $Ca = \mu U/\gamma$. For water, we have Ca ~ 0.01, and for glycerol, Ca ~ 10. Thus, it is expected that surface tension dominates over viscous effects for water and vice versa for glycerol. In Fig. 2a, we show a phase diagram with the different observed scenarios for experiments with water drop impact where the center-to-center hair spacing d and the velocity of impact V is varied. The symbols correspond to the states shown in Fig. 1. For dense hairs, i.e. small values of d, the drop either partially penetrates or penetrates and is captured. The cases where drop spreading or droplet ejection occurs are for lower hair density or higher impact velocity. A similar phase diagram is also shown for experiments with glycerol in Fig. 2b, which is about 1000 times more viscous than water. In these experiments, the drops do not penetrate for high hair density, but penetrate as the space between the hairs increases. For glycerol, drop penetration with spreading or droplet ejection is not observed in the parameter range tested.

Fig. 2c and d show two different experiments in which penetration with capture is observed for water and glycerol, respectively (corresponding videos shown in Supplemental Movies 3 and 6, see Refs. [30, 33]). For the experiment with water in Fig. 2c, $d = 0.75$ mm, and $V = 0.6$ m/s. For the experiment with glycerol in Fig. 2d, the space between the hairs and the speed of impact is higher, with $d = 1.5$ mm and $V = 2.0$ m/s. In both cases the hairs slow the drop sufficiently such that no significant spreading is observed. The same behavior is observed in these two scenarios, but driven by different physical mechanisms, either viscosity or surface tension.

Let us denote $\mathcal{E}_k = \frac{1}{2}\rho V^2 \frac{4}{3}\pi R^3$, the kinetic energy of the impinging drop. In the inviscid regime, Fig. 2a and

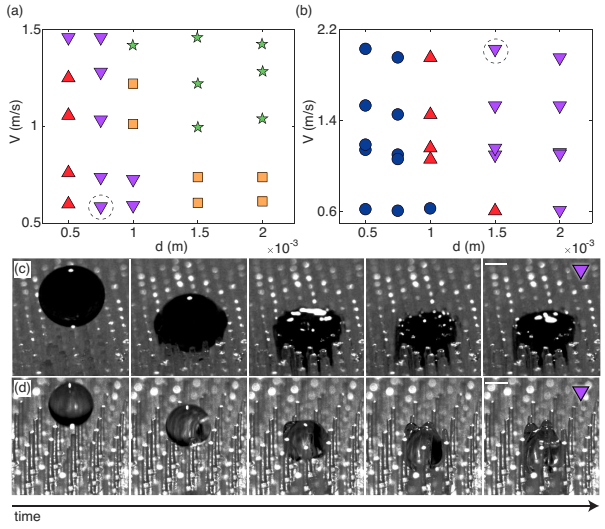

FIG. 2. a) Phase diagram for drop impact experiments with water. Symbols defined in Fig. 1. b) Phase diagram for drop impact experiments with glycerol. Symbols defined in Fig. 1. c) Montage of water drop impact on a hairy surface with d = 0.75 mm. The speed of impact is V = 0.6 m/s. The time interval between frames is 2.8 ms. The corresponding point in the phase diagram a) is surrounded by a dashed circle. d) Montage of glycerol drop impact on a hairy surface with d = 1.5 mm. The speed of impact is V = 2.0 m/s. The time interval between frames is 0.83 ms. The corresponding point in the phase diagram b) is surrounded by a dashed circle. The scale bars indicate 1mm.

c, we expect $\mathcal{E}_k$ to be balanced primarily by capillary forces, while viscous effects are anticipated to dominate the impact dynamics in the viscous limit, Fig. 2b and d. In both cases, we anticipate that the geometrical features of the hairs impose new relevant lengthscales in the problem. We proceed by quantifying the contribution of the hairs to the impact dynamics in the case where the drop penetrates and is captured (Fig. 2c and d). The impact duration is estimated as the time taken for the drop to go from the tip of the hairs to the base plate at velocity V, so that $t_c = \ell/V$, where ℓ is the length of the hairs. The edge-to-edge space between the posts $r = d-2a$ (see Fig. 1a) is much smaller than the size of the drop, and therefore is the relevant length scale in evaluating the viscous dissipation function [10], which here is given by $\mu\left(\frac{V}{r}\right)^2$. In turn, the viscous energy loss is approximated as:

$$\mathcal{E}_v = \frac{4\pi R^3}{3}\int_0^{t_c} \mu\left(\frac{V}{r}\right)^2 dt = \frac{4\pi R^3}{3}\mu\frac{V\ell}{r^2}. \qquad (1)$$

The number of posts under the impinging drop with radius R is $n_p = \frac{R^2}{d^2}\frac{2\pi}{\sqrt{3}}$, with the prefactor arising from the hexagonal arrangement of the hairs (Fig. 1)a). As the drop travels through the hairs, the variation of surface energy due to replacing a solid-gas interface (surface energy γ_{SG}) with a solid-liquid interface (γ_{SL}) is:

$$\mathcal{E}_\gamma = (2\pi a\ell+\pi d^2)(\gamma_{SL}-\gamma_{SG})n_p \simeq (2\pi a\ell+\pi d^2)\gamma\, n_p, \quad (2)$$

where γ is the liquid surface tension and $2\pi a\ell$ is the surface area of a single post. Balancing $\mathcal{E}_k$ with $\mathcal{E}_v$ and balancing $\mathcal{E}_k$ with $\mathcal{E}_\gamma$, yields the modified Reynolds number Re^* and the modified Weber number We^*, respectively:

$$Re^* = \frac{1}{2}\frac{\rho V r^2}{\mu\ell}, \quad We^* = \frac{\rho V^2 R}{\gamma}\frac{\sqrt{3}d^2}{3(2\pi a\ell+\pi d^2)}. \qquad (3)$$

In the captured states depicted in Fig. 2c,d, the kinetic energy of the drop is expended by viscous dissipation and capillary effects, and it is zero when reaching the base plate: $\mathcal{E}_k = \mathcal{E}_v + \mathcal{E}_\gamma$, yielding

$$\frac{1}{Re^*} + \frac{1}{We^*} = 1. \qquad (4)$$

With this relation in hand, and using the modified Reynolds and Weber numbers, we proceed to rationalize our experimental observations.

IV. DISCUSSION

We construct a state diagram using all experimental data, in terms of modified Reynolds and Weber numbers (Fig. 3). The experimental data segregate into clusters. The clusters are organized by their states, and ordered from low to high inertia when traveling from the lower left corner where we observe drops not penetrating to the upper right corner of the plot where we find that the drops penetrate and break apart. These two limit cases correspond to ($Re^* \ll 1, We^* \ll 1$) where viscosity and surface tension dominate over inertia and ($Re^* \gg 1, We^* \gg 1$) where inertia dominates. The central cluster of points labeled $\bigtriangledown$ corresponds to the case, shown Fig 2c,d, where the drop is captured in the hair texture. We find that Eq. 4 sits among the points of the cluster as anticipated (plotted as a solid black line Fig. 3). We now use this reference case to obtain the boundaries between all states using scaling arguments.

We define $\beta = (\mathcal{E}_v + \mathcal{E}_\gamma)/\mathcal{E}_k$, the ratio between the energy lost by passing through the hair and the kinetic energy of the impinging drop as expressed using Eq. 1 and 2, and the kinetic energy of the drop $\mathcal{E}_k$. This balance can be expressed in terms of the modified Reynolds and Weber numbers as $\frac{1}{Re^*} + \frac{1}{We^*} = \beta$. In the capture case, we have $\beta = 1$. In other cases, the kinetic energy may be in excess, $\beta < 1$ so that the drop reaches the bottom plate with non-zero speed, or insufficient $\beta > 1$ so that the drop stops before reaching the base plate. Following this reasoning, we find that the values $\beta = 0.2, 0.5, 1$ and 5 fit the boundaries between the various states in Figure 3.

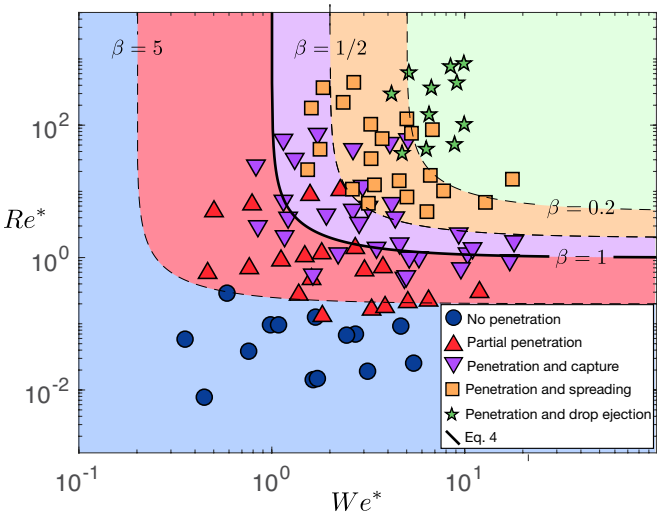

FIG. 3. Phase diagram: Shown on the diagram are the various possible states observed in our experiments. Data is plotted in the (Re^*, We^*) phase space, as defined in Eq.3. Superimposed on the diagram are the lines obtained by the balance of energy yielding Eq. 4. The dotted lines correspond to the values of $\beta = 0.2, 0.5, 1$ and 5. These isolines are obtained using Eq. 4 and form boundaries between the observed states.

These boundaries are produced by substituting the corresponding values of β for 1 in Eq. 4. They correspond to isolines of dimensionless kinetic energy in the (Re^*, We^*) phase space. The isolines and the experimental data are shown in Fig. 3.

In the remainder of this paper, we discuss the merits and limitations of our approach. Impacts of drops on flat surfaces are complex, exhibiting a myriad of regimes depending on the properties of the substrate, the fluid and the impact parameters. The presence of hair adds to this complexity, so that approximations are necessary to model this system under a unified framework. Our approximations hinge on the capture case, specifically on the fact that neither the drop, nor the hair significantly deform in this case, facilitating our analysis. In this simple case we only need to consider the viscous dissipation and surface tension effects originating from the interaction with the hair. Deformation of the drop itself and of the hair are neglected, although they do appear in other states. We argue that the reference state is sufficient to estimate the boundaries of other states through scaling arguments, although the model does not include the finer details of these states.

If the kinetic energy of the drop is larger than the dissipation due to the hair, $\beta < 1$, we expect the drop to spread on the base plate. The spreading drops will push past the posts and form fingers when $\beta \ll 1$. Our results are in agreements with these estimates as the boundary between $\bigtriangledown$ and $\square$ in Figure 3 is found for $\beta \simeq 0.5$ and the boundary between $\square$ and $\bigstar$ is found for $\beta \simeq 0.2$. Similarly, if the kinetic energy of the drop is smaller than the dissipation due to the hair, $\beta = >1$ we expect the drop to only partially penetrate the hair as the drop should come to rest before it reaches the bottom plate. Our results are in agreements with these estimates as the boundary between $\bigtriangledown$ and $\bigtriangleup$ in Figure 3 is found for $\beta \simeq 1$. Our model assumes that kinetic energy is dissipated through contact with the hairs. However, for the case of small kinetic energy, $\beta \gg 1$, we find that the drop does not penetrate the hairs at all and the kinetic energy is fully dissipated due to the high viscosity and deformation of the drop itself.

In the case of high kinetic energy, $\beta \ll 1$, we observe the drop forming fingers as it pushes past the posts. The creation of these fingers should lead to an increase in viscous dissipation and surface energy, which is beyond the scope of this study, but an interesting topic for further investigation.

ACKNOWLEDGMENTS

A.N. and A.E.H. acknowledge support from the U. S. Army Research Office under grant number ARO W911NF-15-1-0166.

[1] D Richard and D Quéré. Bouncing water drops. *EPL (Europhysics Letters)*, 50(6):769, 2000.

[2] M Reyssat, A Pépin, F Marty, Y Chen, and D Quéré. Bouncing transitions on microtextured materials. *EPL (Europhysics Letters)*, 74(2):306, 2006.

[3] Christophe Clanet, Cédric Béguin, Denis Richard, and David Quéré. Maximal deformation of an impacting drop. *Journal of Fluid Mechanics*, 517:199–208, 2004.

[4] Yongmei Zheng, Xuefeng Gao, and Lei Jiang. Directional adhesion of superhydrophobic butterfly wings. *Soft Matter*, 3(2):178–182, 2007.

[5] Wilhelm Barthlott and Christoph Neinhuis. Purity of the sacred lotus, or escape from contamination in biological surfaces. *Planta*, 202(1):1–8, 1997.

[6] Lidiya Mishchenko, Benjamin Hatton, Vaibhav Bahadur, J Ashley Taylor, Tom Krupenkin, and Joanna Aizenberg. Design of ice-free nanostructured surfaces based on repulsion of impacting water droplets. *ACS nano*, 4(12):7699–7707, 2010.

[7] James C Bird, Rajeev Dhiman, Hyuk-Min Kwon, and Kripa K Varanasi. Reducing the contact time of a bouncing drop. *Nature*, 503(7476):385, 2013.

[8] Jonathan B Boreyko and Chuan-Hua Chen. Self-propelled dropwise condensate on superhydrophobic surfaces. *Physical review letters*, 103(18):184501, 2009.

[9] Katrina M Wisdom, Jolanta A Watson, Xiaopeng Qu, Fangjie Liu, Gregory S Watson, and Chuan-Hua Chen. Self-cleaning of superhydrophobic surfaces by self-

propelled jumping condensate. *Proceedings of the National Academy of Sciences*, 110(20):7992–7997, 2013.

[10] S Chandra and CT Avedisian. On the collision of a droplet with a solid surface. *Proc. R. Soc. Lond. A*, 432(1884):13–41, 1991.

[11] Peichun Tsai, Sergio Pacheco, Christophe Pirat, Leon Lefferts, and Detlef Lohse. Drop impact upon micro-and nanostructured superhydrophobic surfaces. *Langmuir*, 25(20):12293–12298, 2009.

[12] Anaïs Gauthier, Sean Symon, Christophe Clanet, and David Quéré. Water impacting on superhydrophobic macrotextures. *Nature communications*, 6:8001, 2015.

[13] Seunggeol Ryu, Prosenjit Sen, Youngsuk Nam, and Choongyeop Lee. Water penetration through a superhydrophobic mesh during a drop impact. *Physical review letters*, 118(1):014501, 2017.

[14] Gannian Zhang, Miguel A Quetzeri-Santiago, Corinne A Stone, Lorenzo Botto, and J Rafael Castrejón-Pita. Droplet impact dynamics on textiles. *Soft matter*, 2018.

[15] Élise Lorenceau and David Quéré. Drops impacting a sieve. *Journal of colloid and interface science*, 263(1):244–249, 2003.

[16] Tristan Gilet and Lydia Bourouiba. Fluid fragmentation shapes rain-induced foliar disease transmission. *Journal of the Royal Society Interface*, 12(104):20141092, 2015.

[17] Jean Comtet, Bavand Keshavarz, and John WM Bush. Drop impact and capture on a thin flexible fiber. *Soft matter*, 12(1):149–156, 2016.

[18] Thomas M Schutzius, Gustav Graeber, Mohamed Elsharkawy, James Oreluk, and Constantine M Megaridis. Morphing and vectoring impacting droplets by means of wettability-engineered surfaces. *Scientific reports*, 4:7029, 2014.

[19] HG Andrews, EA Eccles, WCE Schofield, and JPS Badyal. Three-dimensional hierarchical structures for fog harvesting. *Langmuir*, 27(7):3798–3802, 2011.

[20] Jie Ju, Hao Bai, Yongmei Zheng, Tianyi Zhao, Ruochen Fang, and Lei Jiang. A multi-structural and multifunctional integrated fog collection system in cactus. *Nature communications*, 3:1247, 2012.

[21] Zhao Pan, William G Pitt, Yuanming Zhang, Nan Wu, Ye Tao, and Tadd T Truscott. The upside-down water collection system of syntrichia caninervis. *Nature plants*, 2:16076, 2016.

[22] Kyoo-Chul Park, Shreerang S Chhatre, Siddarth Srinivasan, Robert E Cohen, and Gareth H McKinley. Optimal design of permeable fiber network structures for fog harvesting. *Langmuir*, 29(43):13269–13277, 2013.

[23] Otto Klemm, Robert S Schemenauer, Anne Lummerich, Pilar Cereceda, Victoria Marzol, David Corell, Johan Van Heerden, Dirk Reinhard, Tseggai Gherezghiher, Jana Olivier, et al. Fog as a fresh-water resource: overview and perspectives. *Ambio*, 41(3):221–234, 2012.

[24] Robert S Schemenauer and Pilar Cereceda. A proposed standard fog collector for use in high-elevation regions. *Journal of Applied Meteorology*, 33(11):1313–1322, 1994.

[25] Ed Ramirez. Urinal splash guard employing flexible bristles. US 2007/0266486A1, November 2007.

[26] Alice Nasto, Marianne Regli, P-T Brun, José Alvarado, Christophe Clanet, and AE Hosoi. Air entrainment in hairy surfaces. *Physical Review Fluids*, 1(3):033905, 2016.

[27] See Supplemental Material at [URL will be inserted by publisher] for a movie of a drop that does not penetrate the hairy texture on impact.

[28] ABD Cassie and S Baxter. Wettability of porous surfaces. *Transactions of the Faraday Society*, 40:546–551, 1944.

[29] See Supplemental Material at [URL will be inserted by publisher] for a movie of a drop that partially penetrates the hairy texture on impact.

[30] See Supplemental Material at [URL will be inserted by publisher] for a movie of a water drop that penetrates through the texture that is "captured," which we define as not spreading beyond the hairs that the drop touches at the moment of impact.

[31] See Supplemental Material at [URL will be inserted by publisher] for a movie of a drop that can spread past the hairs on impact but remains as one drop.

[32] See Supplemental Material at [URL will be inserted by publisher] for a movie of a drop that forms fingers as it pushes between hairs and breaks up into multiple droplets.

[33] See Supplemental Material at [URL will be inserted by publisher] for a movie of a glycerol drop that penetrates through the texture that is captured.